

Simulating dynamic processes and hypermobility mechanisms of the Wenjiagou rock avalanche triggered by the 2008 Wenchuan earthquake using discrete element modelling

Qinghai Deng¹ · Linxian Gong¹ · Liping Zhang¹ · Renmao Yuan² ·
Yongqiang Xue¹ · Xuke Geng¹ · Shanxiang Hu¹

Received: 29 December 2015 / Accepted: 25 June 2016 / Published online: 8 July 2016
© Springer-Verlag Berlin Heidelberg 2016

Abstract The discrete element method is well suited for simulating the cracks and subsequent large displacements of catastrophic landslides or rock avalanches, and is therefore a useful tool for analysing their complicated dynamic processes and hypermobility mechanisms. In this study, particle flow code was used to investigate the dynamic processes and hypermobility mechanisms of the Wenjiagou rock avalanche triggered by the 2008 Wenchuan earthquake. Characterization of the avalanche dynamics was achieved using a model comprising four stages: failure rupture, projectile motion, granular debris flow, and debris mass accumulation. The results show that collision on the valley floor was the main factor causing the fragmentation of the Wenjiagou rock avalanche. The upper and front edge of the landslide body were the most likely to move over a long distance. The results also show that friction was the main source of energy dissipation during the entirety of the avalanche movement. The high gravitational potential energy of the avalanche was the basis of the high mobility. In addition, because of their effects on energy dissipation, the low basal friction coefficient, favourable block movement, and topographical conditions played key roles in the rapid, long-runout Wenjiagou avalanche process.

Keywords Wenjiagou rock avalanche · Discrete element method · Dynamic processes · Hypermobility mechanisms · 2008 Wenchuan earthquake

Introduction

A long-runout rock avalanche is defined as an extremely rapid, massive, flow-like motion of fragmented rock derived from a bedrock failure, which exhibits much greater mobility than could be predicted using frictional models (Hung et al. 2001; Dufresne and Davies 2009). The 2008 magnitude-7.9 Wenchuan earthquake in China triggered hundreds of rapid long-runout rock avalanches, causing over 20,000 casualties (Yin et al. 2009). In light of the potential devastating effects of such events, it is important to understand the dynamic processes and hypermobility mechanisms of long-runout rock avalanches in order to improve hazard prevention and mitigation measures (Zhang et al. 2011).

The avalanching process is extremely complicated, and it is rarely monitored in the field because of the suddenness of the failure and extremely rapid motion (Zhang and Yin 2013; Zhang et al. 2016). Generally, dynamic rock avalanches can be divided into three consecutive phases: detachment, disintegration, and flow. The disintegration phase that links the detachment and flow, however, is still poorly understood. Therefore, understanding the importance of disintegration and the effect of site conditions on fluidization and mobilization is helpful for a better understanding of the avalanche mechanisms (Knapp et al. 2015).

The high-mobility mechanism of rock avalanches is a topic that has garnered much attention. Many models have been proposed for discussing the hypermobility of rock avalanches. These include entrapped and compressed air

✉ Qinghai Deng
dqh5027@163.com

¹ Shandong Provincial Key Laboratory of Depositional Mineralization and Sedimentary Minerals, College of Earth Science and Engineering, Shandong University of Science and Technology, No. 579, Qianwangang Road, Hungdao District, Qingdao 266590, People's Republic of China

² Key Laboratory of Active Tectonics and Volcano, China Earthquake Administration, Institute of Geology, Beijing 100029, People's Republic of China

(Kent 1966), air-layer lubrication (Shreve 1966), grain flow (Hsü 1975), low-friction sliding on a dissociated or melted rock layer (Erismann 1979), mechanical fluidization (Davies 1982), momentum transfer (Davies et al. 1999; Eisbacher 1979; Okura et al. 2000), and pore water hypotheses (Deline 2009). At the same time, statistical relationships have been identified between mobility and the factors (e.g. the volume and the equivalent coefficient of friction) that influence the rock avalanche (Hsü 1975; Nicoletti and Sorriso-Valvo 1991; Okura et al. 2000). However, the hypotheses on which these models and relationships are based are extremely difficult to verify or refute with confidence, because of the difficulty in measuring the dynamic transport parameters of rock avalanches (Zhang et al. 2016).

Field investigations, laboratory tests, and numerical simulations can all be used to analyse the dynamic problems of rock avalanches (Ayotte and Hungr 2000). Field investigations can provide evidence of the dynamic processes, but cannot determine the time process of landslides (Zhou et al. 2015). Empirical methods are easy to apply but lack robustness because of the complicated geological and geotechnical conditions applicable to rock avalanches (Legros 2002). In contrast, the numerical simulation technique provides an appropriate and useful tool for modelling the dynamic process of rock avalanches. Numerical landslide models include two major categories: continuum models and discrete element models. The continuum method, based on fluid mechanics, such as the smoothed particle hydrodynamics (SPH) model, is able to simulate the propagation of rock avalanches (Huang et al. 2012, 2015b). Traditional continuum-based numerical models often fail to reproduce the progressive failure of rock slopes, especially the dynamics of kinematic release accompanying complex internal distortion, dilation, and fracture (Stead et al. 2006). Unlike the traditional models, the particle flow code (PFC), which is based on the discrete element method (DEM), does not limit the scale of separation and displacement behaviours of elements, and the movement process of the mass from fracture to separation can be fully simulated. It is therefore an effective tool for robustly modelling the avalanching process (Poisel and Roth 2004). The DEM PFC has been used to simulate the large displacements of catastrophic landslides (e.g. Lo et al. 2011, 2014; Lu et al. 2014; Poisel et al. 2008; Tang et al. 2009; Thompson et al. 2009; Yuan et al. 2014; Zhou et al. 2013).

The 2008 Mw 7.9 Wenchuan earthquake induced extremely large landslide events in the Longmenshan area of China. One such event was the Wenjiagou rock avalanche in Qingping County, Mianzhu, China—a typical high-speed and long-runout landslide that caused 48 deaths. After the landslide event, a few field investigations

and analyses were carried out to gain an understanding of its initiation and propagation mechanisms (Huang et al. 2015a; Tang et al. 2015; Zhang et al. 2016). However, because of the complex motion involved, the dynamic processes and hypermobility mechanisms of the Wenjiagou rock avalanche remain poorly understood. In this paper, we use the two-dimensional discrete element code PFC2D from Itasca Consulting Group to characterize the complex kinematics and highly unusual mobility mechanism of the Wenjiagou rock avalanche.

The Wenjiagou avalanche

Features of the Wenjiagou area

During the 2008 Wenchuan earthquake, dozens of huge landslides were triggered along the Longmenshan fault zone, which is the collision area between the Tibetan Plateau and the Sichuan Basin (Fig. 1). Wenjiagou Valley, an E–W deep-cut gully, lies on the left bank of the Mianyuan River in Qingping Town, Mianzhu City, Sichuan Province, China (104°25′56.93″E, 31°50′40.60″N) (Fig. 1). The distance between the valley and the Longmenshan earthquake fault is only 3.6 km. Folds and faults are well developed in this area and disrupt the continuity and integrity of the original formation. Topographically, the Wenjiagou area is characterized by low mountains and hills. The lowest elevation of the Wenjiagou gully is about 890 m, while the elevation of the watershed is 2402 m, and thus the difference in elevation is very large (1512 m). The peak of the eastern ridge, Dingziya, has a fan-shaped upper gully and average slope of 45° (Wu et al. 2010). The combination of geological and topographical features makes the area susceptible to landslides (Huang et al. 2015a).

The 2008 Wenjiagou rock avalanche

The earthquake-triggered Wenjiagou rock avalanche had an initial volume of 27.5 million m³, and ran over 1360 m vertically and 4170 m horizontally within about 2 min. The avalanche can be divided into three areas: source area, acceleration area, and deposition area (Figs. 2, 3, 4b). Before the event, the Wenjiagou mountain was covered in rich vegetation (Fig. 4a), and the D_{2g} carbonate rock mass in the landslide source area was stable according to field investigations and remote sensing. The bedrock of the Wenjiagou rock avalanche comprised Qingping formation (ϵ_{1qp}) sandstone and Guanwushan formation (D_{2g}) limestone, separated by the Dingziya Fault (Fig. 3). The source area of the rock avalanche was between 1850 and 2200 m in elevation.

Fig. 1 Location of the Wenjiagou rock avalanche and surface ruptures in the 2008 Wenchuan earthquake

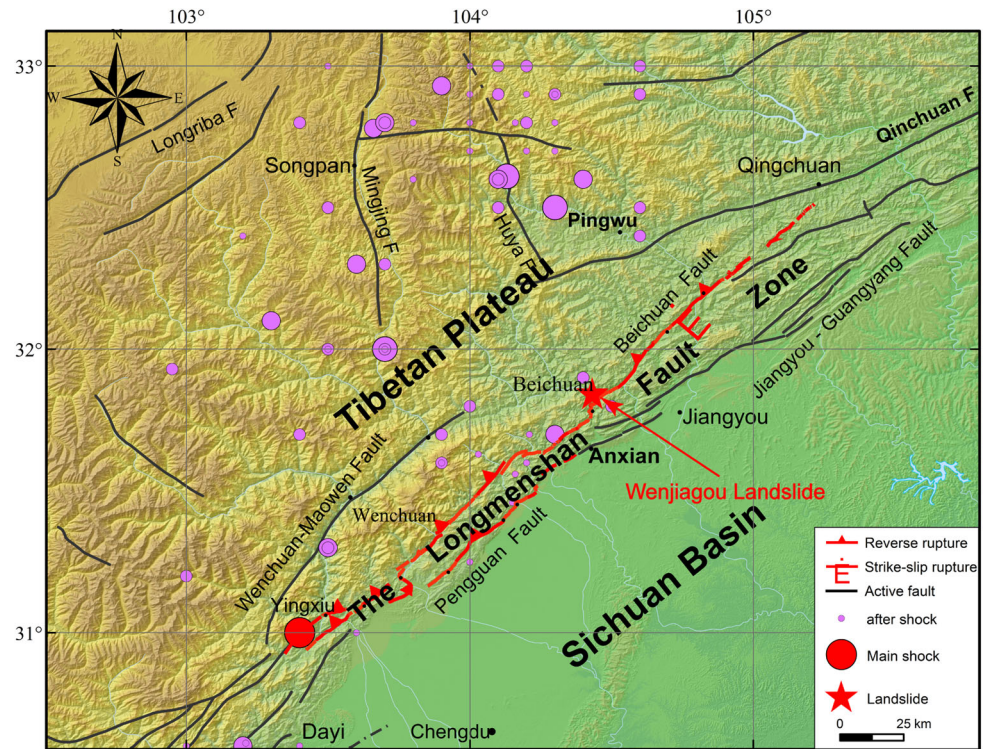
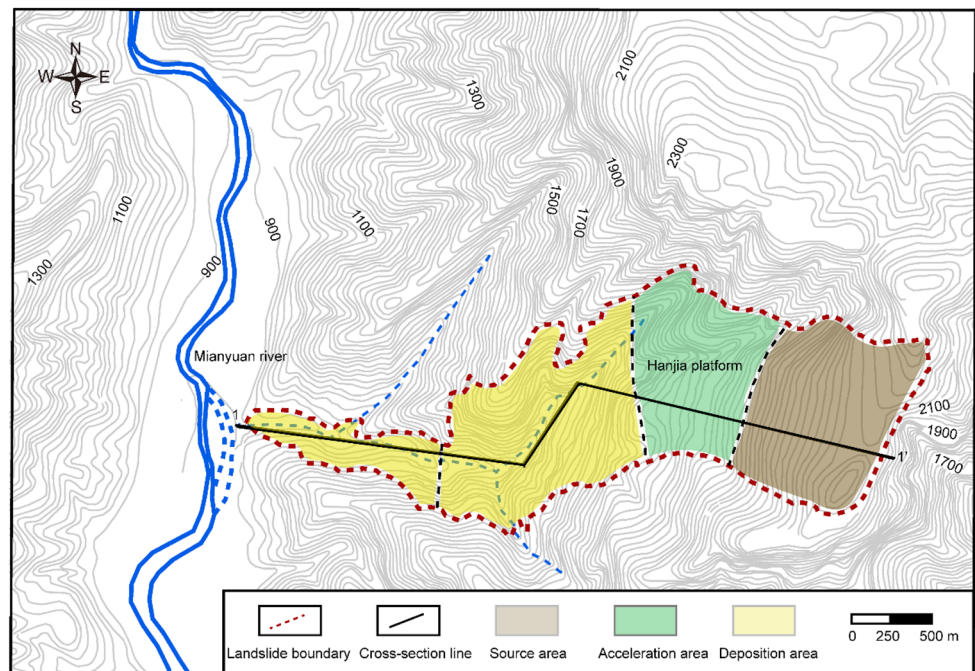


Fig. 2 A plan view of the Wenjiagou rock avalanche



The rock mass in the source area was largely composed of weak weathered limestone and dolomitic limestone. The main scarp was 445 m high, and was formed of jointed dolomite (Fig. 5). Karst erosion had caused widespread development of holes and other structural defects in the limestone rock body.

During the 2008 Wenchuan earthquake, the rock slope was severely shaken, and strong ground acceleration led to slope failure. Subsequently, the dip slope rock mass slid at high speed over a short period of time from the source area, running out from the top of a 280-m cliff, and landing in the other side of the valley. When this rock

Fig. 3 Longitudinal section of the Wenjiagou rock avalanche

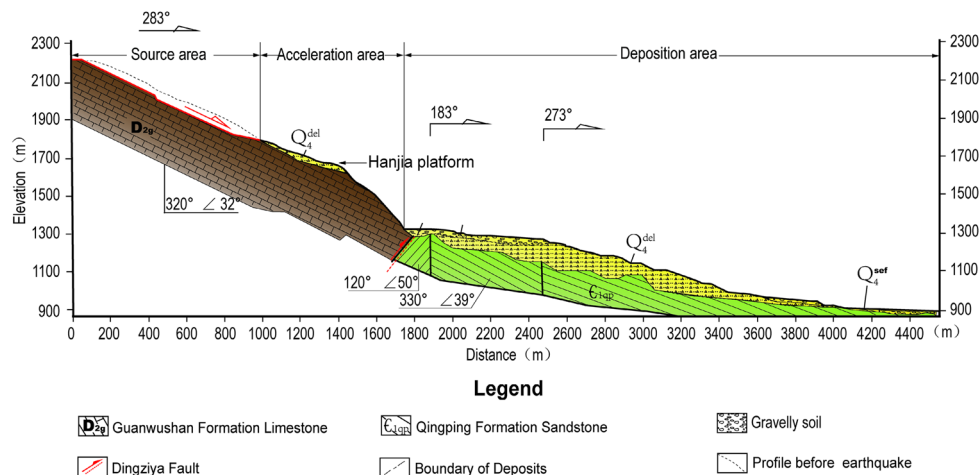


Fig. 4 **a** The pre-seismic and **b** post-seismic three-dimensional visualization of the Wenjiagou area (Liang 2014)

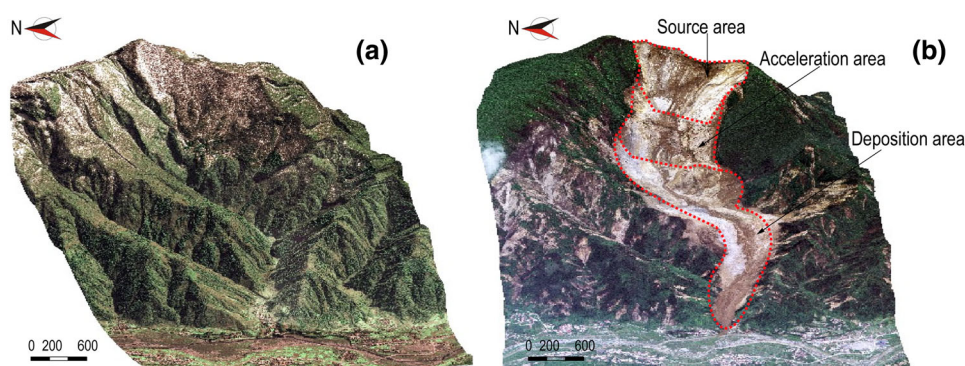


Fig. 5 The main scarp of the Wenjiagou rock avalanche

mass collided with a ridge on the right bank of the gully, the mass transformed to a debris-flow avalanche. A powerful air blast induced by the displaced material destroyed original fir forests along its travel path, indicating the high-speed movement of the rock avalanche. The fragmented rock debris then travelled along the Wenjiagou Valley at very high velocities, and came to a stop near the entrance of the valley. The original V-shaped valley was thus carved into the current U-shaped valley (Fig. 4). Most of the Wenjiagou landslide

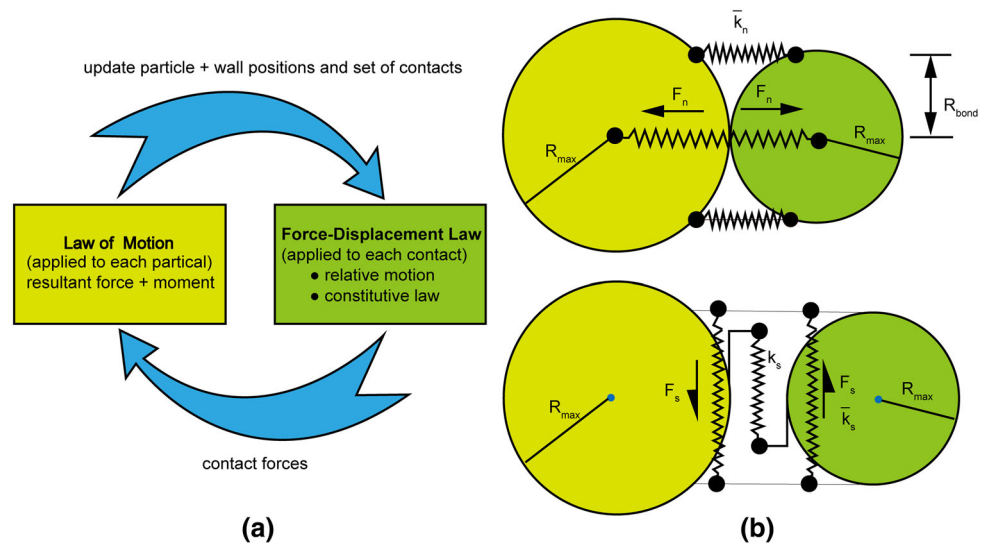
deposits consisted of angular blocks of limestone and dolomitic limestone gravel, but included some sandstone from adjacent mountains. The debris avalanche deposits were poorly sorted. The maximum deposit thickness was about 150 m and the total volume of the deposits was approximately 50 million m^3 . The abundant loose solid material produced by the Wenjiagou rock avalanche was easily transformed into debris flows by subsequent heavy rainfall. On August 13, 2010, a heavy rainstorm in Wenjiagou Valley triggered a catastrophic debris flow, with total volume of $3.1 \times 10^6 m^3$.

In this work, the PFC2D based on the DEM is used to simulate the Wenjiagou avalanche in order to analyse its dynamic processes and mechanisms.

The discrete element method

The PFC model was first developed for the analysis of a system of rock blocks (Cundall 1971), and it was later applied to study the behaviour of granular materials (Cundall and Strack 1979). The PFC (2D and 3D) provides two basic elements: balls and walls. The calculation cycle performed in PFC is a time-stepping algorithm (Fig. 6a). At

Fig. 6 **a** The calculated cycle in the PFC model; **b** the schematic diagram of parallel bond used in the PFC model



the beginning of every time step, the set of contacts is updated from the known particle and wall positions. The force–displacement law is then applied to each contact to update the contact forces, and the law of motion is then applied to each particle to update its velocity and position. In addition, the wall positions are updated based on the specified wall velocities.

Based on this method, an assembly of circular particles in the PFC is connected by a network of contacts. The overall constitutive behaviour of a material is simulated by associating a simple constitutive model with each contact. The constitutive model acting at a particular contact consists of three parts: a stiffness model, a slip model, and a bonding model. The parallel bond model can be used to describe the constitutive relation of the cementing material within a limited range of particles and to transmit force and moment (Fig. 6b). The corresponding force and moment produced by the relative displacement of the parallel bond will be imposed on the two connected particles as a counterforce. When one of the maximum stresses exceeds its corresponding bonded strength, the parallel bond breaks.

Numerical modelling of the Wenjiagou landslide

Numerical model

The slope geometry and geologic structure of the two-dimensional model is based on the geological longitudinal section through the Wenjiagou Valley (Fig. 3). The sliding surface of the numerical model is represented by wall elements. The sliding body is constructed using 8000 ball elements with radiuses of 1.5–2.5 m (Fig. 7). To track the velocity and displacement of different parts of the

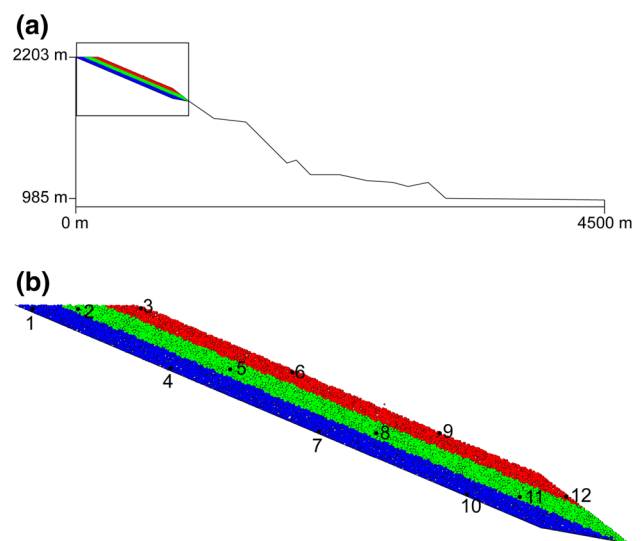


Fig. 7 **a** Numerical model created by PFC2D and **b** monitored particles in the PFC model

Wenjiagou rock avalanche during the earthquake, 12 particles in the model are monitored as shown in Fig. 7b.

Model parameters

Microscopic parameters

To enable the use of PFC models as a reliable simulation tool, it is necessary to establish reasonable relations between the numerical parameters and the mechanical characteristics of real problems (Potyondy and Cundall 2004). The parameters needed in the continuum-based numerical models are at a macro level and can be derived directly from measurements performed on laboratory

specimens. The parameters required in the PFC2D, however, are at a micro level, and can only be correlated in interactions between particles. Since there is still no reliable or generally accepted theory that describes the relationships between the macro and micro parameters, a trial-and-error calibration was applied to determine micro-level parameters for the PFC2D. Figure 8 presents the calibration procedure that was used to induce the PFC2D grain-based model to adequately reproduce the mechanical behaviours of the target rock mass. In this study, the calibrated target values, such as the compressive strength and deformation modulus properties of large-scale rock masses for landslide simulation, were derived using the Hoek–Brown failure criterion. During the process of trial and error, the target values calculated from the DEM simulations were adjusted to match the macroscopic response of physical experiments such as uniaxial compressive tests.

In rock mechanics, the Hoek–Brown criterion is generally applied for estimating the strength of large-scale rock masses. Therefore, this criterion is suitable for studying the kinetic behaviours of rock avalanches. In this study, the most recent version of the Hoek–Brown failure criterion (Hoek et al. 2002) is employed:

$$\sigma'_1 = \sigma'_3 + \sigma_{ci} \left(m_b \frac{\sigma'_3}{\sigma_{ci}} + s \right)^a, \tag{1}$$

where σ'_1 and σ'_3 are the maximum and minimum effective principal stress, respectively, σ_{ci} is the uniaxial compressive strength of the intact rock, m_b is the modified Hoek–Brown constant for the rock mass, and s and a are property-dependent constants.

To apply the Hoek–Brown failure criterion, the value of m_i can be used to determine the modified values m_b , s and a as given by the equations of Hoek 2002:

$$m_b = m_i \left(\frac{GSI - 100}{28 - 14D} \right), \tag{2}$$

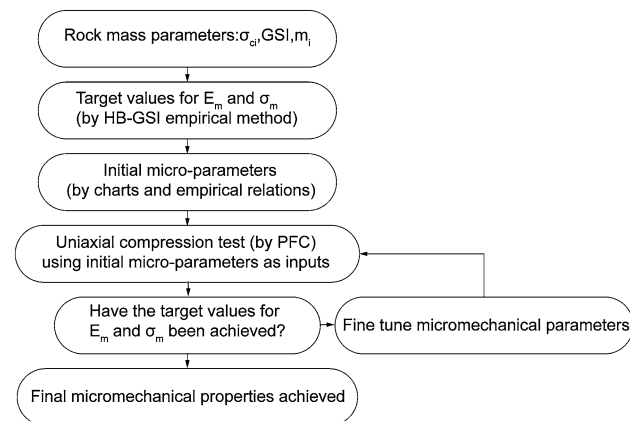


Fig. 8 PFC model calibration procedure (modified from Saiang 2008)

$$s = \exp\left(\frac{GSI - 100}{9 - 3D}\right), \tag{3}$$

$$a = \frac{1}{2} + \frac{1}{6} \left(e^{-GSI/15} - e^{-\frac{20}{3}} \right), \tag{4}$$

where m_i is the Hoek–Brown constant for the intact rock, D is the disturbance factor, and GSI is the Geological Strength Index.

Hoek (Hoek 1994; Hoek et al. 2002) provided the guidelines on the selection of D and GSI .

The uniaxial compressive strength of the Hoek–Brown model is obtained by setting σ_3' in Eq. (1):

$$\sigma_m = \sigma_{ci}(s)^a. \tag{5}$$

The generalized Hoek and Diederichs equation (Hoek and Diederichs 2006) utilizes the intact rock modulus as well as GSI and D to compute the rock mass modulus. The modulus is calculated in MPa:

$$E_m = E_i \left(0.02 + \frac{1 - D/2}{1 + e^{((60+15D-GSI)/11)}} \right), \tag{6}$$

where E_m is the rock mass deformation modulus, and E_i is the intact rock deformation modulus.

A series of numerical uniaxial compressive tests were then performed on cemented granular samples to obtain the closest match to target values using the Hoek–Brown Geological Strength Index empirical method. The 2D cylindrical specimen had a height of 400 mm and a diameter of 200 mm, and consisted of 4000 rigid disks. Fine-tuning of the micro-mechanical parameters was achieved by repeating uniaxial compression tests on the specimens until the target values computed from the stress–strain curve (Fig. 9) were obtained. As shown in Table 1, the resulting values from the numerical model are very close to the properties of the rock mass of the Guanwushan formation limestone, as determined from the Hoek–Brown criterion. Table 2 shows the calibrated set of parameters for modelling the mass movement of the Wenjiagou rock avalanche using PFC2D.

Numerical damping

Particular attention was paid to calibrating the numerical damping parameter, which is the only parameter that cannot be explicitly related to any physical mechanism. The damping coefficient can have a significant impact on the results (Thompson et al. 2009). Local damping is available in PFC2D to dissipate energy by effectively damping the governing equation of motion. However, local damping is not applicable for landslide simulation. Viscous damping uses a spring-dashpot system and adds normal and shear dashpots at each contact. The parameter of viscous damping in PFC2D can also influence the motion of grains

Fig. 9 Uniaxial compressive test model and stress–strain curve

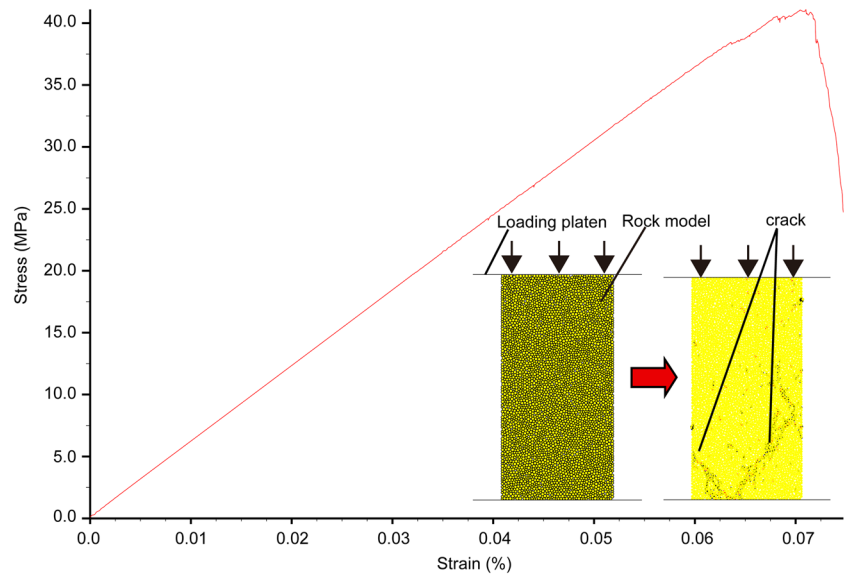


Table 1 Comparison of numerical simulation results and results estimated by Hoek–Brown

Parameters	Hoek–Brown	PFC2D
Young’s modulus (Gpa)	58.5	58
Poisson’s ratio	0.23	0.21
Unconfined compressive strength (Mpa)	42	41

Table 2 Micro-mechanical parameters for computation

Parameters	Value
Minimum ball radius (m)	1.5
Ball size ratio	1.66
Ball density (kg/m ³)	2720
Ball–ball contact modulus (Gpa)	54
Ball normal/shear stiffness ratio	2.50
Ball friction coefficient	0.50
Parallel bond normal/shear stiffness ratio	2.50
Parallel bond normal strength (Mpa)	41
Parallel bond shear strength (Mpa)	41
Parallel bond modulus (Gpa)	54
Parallel bond radius multiplier	1
Normal stiffness of balls (N/m)	5.2e10
Parallel bond normal stiffness (N/m)	1.3e10
Normal and shear stiffness of walls (N/m)	1e12

and reflect energy dissipation during collision. The damping parameters are correlated with the coefficients of restitution, which can be measured in the laboratory or field. This study used the results of restitution coefficient tests in the field by Giani (1992) to define damping

parameters (Table 3). The values of the normal and shear damping coefficients are thus set at 0.4 and 0.2, respectively.

Boundary conditions

After a primary stress field caused by gravity load was generated, seismic motion was applied to the wall boundary by integrating the corrected accelerations recorded at the Qingping seismic station during the Wenchuan earthquake. A seismic shaking duration of 150 s was adopted in this study. Ground motion amplification may have occurred at the mountain crest in the low-frequency domain (Havenith et al. 2003). Therefore, triggering of the Wenjiagou rock avalanche was likely facilitated by the amplification of seismic waves. In view of the upscaling of the topography effect in this area, the value of the amplification factor was taken as 3.0 (Yuan et al. 2010). The resultant horizontal and vertical velocity time histories along the slide direction of the Wenjiagou landslide are used in the model (Fig. 10).

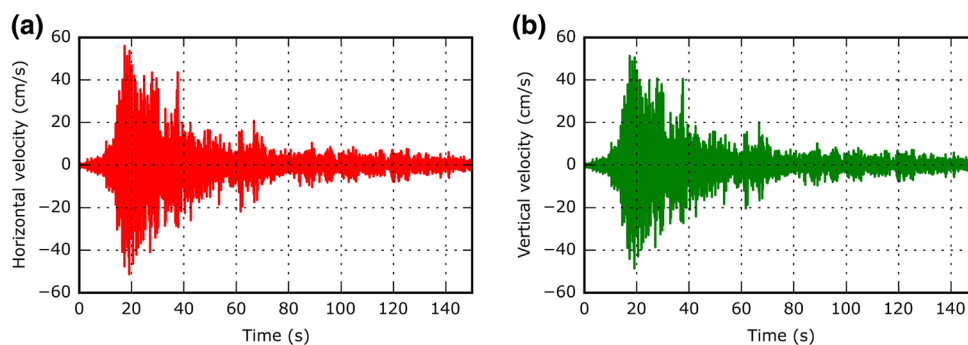
Results and discussion

Dynamic process of mass movement

A visual presentation of the dynamic process of the Wenjiagou rock avalanche is provided in Fig. 11, which shows the state of the rock mass at different stages. The evolution of the avalanche can be divided into four dynamic segments: failure rupture, projectile motion, granular debris flow, and debris mass accumulation.

Table 3 The relationship between coefficient of restitution and damping ratio by rockfall test in the field (modified from Giani 1992)

Slope materials	Normal restitution coefficient	Normal damping ratio	Shear restitution coefficient	Shear damping ratio
Bedrock	0.5	0.21	0.95	0.02
Bedrock covered by large blocks	0.35	0.32	0.85	0.05
Rock debris and soil	0.3	0.36	0.70	0.11
Soil covered by vegetation	0.25	0.40	0.55	0.20

Fig. 10 The original time history seismic curves

Failure rupture process

In the initial stage of the Wenjiagou rock avalanche, a rock slide occurred. The development of cracks or fissures in the rock mass, induced under shaking and sliding, can be observed (Fig. 11a). Under earthquake excitement, tensile cracks were initiated on the surface of the rock mass, forming a tensile stress concentration zone. The cracks then widened laterally and propagated vertically to the detachment surface, generating the horizontal and vertical displacements. After about 20 s, the avalanche mass was fully separated and began to slide rapidly down the slope surface at its initial speed (Fig. 11b). In addition to the trigger of violent quaking, the relatively steeply dipping hill slope facilitated the rockslide.

Projectile motion

Under seismic and gravity forces, the avalanche mass achieved a high initial speed of about 30 m/s (Fig. 12) over a short period as it moved down the basal surface (Fig. 11b). When the upper sliding body reached a steep cliff, an ejection phenomenon occurred (Fig. 11c, d), wherein the sliding body ran out from the top of the 280-m cliff, flying along a parabolic path. While undergoing projectile motion, the rock avalanche accelerated rapidly (Fig. 12). A highly probable interpretation is that the high initial velocity and the large difference in elevation between the cliff and the valley bottom induced the projectile motion.

Granular debris flow

After the ejected body had flown through the air, it collided with the valley floor at speeds of about 40–50 m/s (Fig. 12) and broke into fragments, which ultimately formed granular debris. The granular debris moved rapidly forward on the valley floor and acted as a flow-like avalanche (Fig. 11e). The speed of movement then began to gradually decrease (Fig. 12), and the flow-like avalanche came to a rest spontaneously after about 120 s (Fig. 12).

Debris mass accumulation

The overall deposition area, stratigraphic sequence, and deposition volume are depicted in Fig. 11f. According to the simulation results, parts of the debris mass accumulated at an elevation of 1000–1100 m, and the others were deposited at an elevation greater than 1100 m. The particles were marked with different colours to simulate the different layers of the original strata, and thus the movement of the different layers can be observed. The deposition at greater than 1100-m elevation clearly shows mostly blue particles in the lower portion and red particles in the upper portion, which is similar to the original layer distribution (Fig. 7b). However, the debris mass that accumulated at an elevation of 1000–1100 m was very disturbed. In addition, the total volume of sturzstrom deposit was more than the initial volume, because of fragmentation of the sliding rock mass and the shovel-scape effect. The sliding surface in the numerical model was represented by wall elements, and so the shovel-scape effect cannot be observed here.

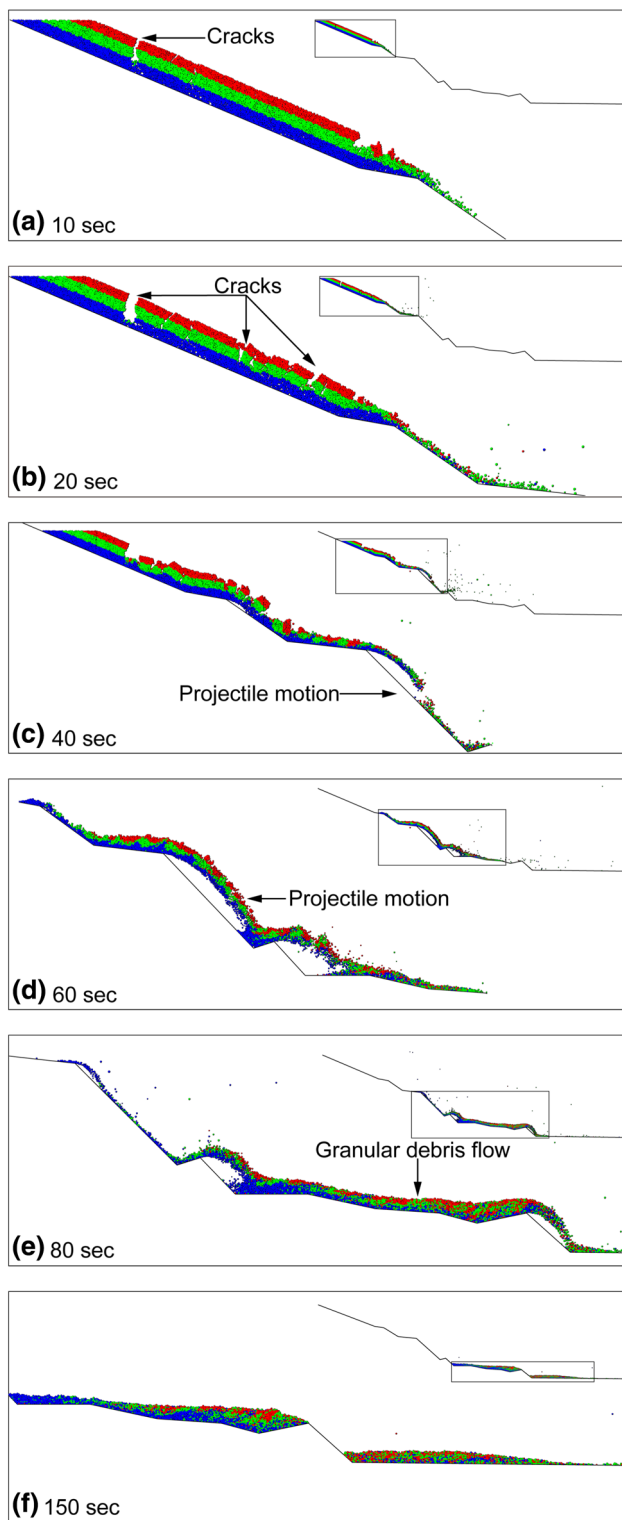


Fig. 11 Wenjiagou landslide simulation scenarios

Variations in velocity and horizontal displacement

In a failure occurrence, the velocities and paths of different points are key factors affecting avalanche dynamics.

Figure 12 shows velocity changes in the monitored particles over time. During the first 20 s, the velocities of the monitored particles were almost zero. At about 20–40 s, their movement was synchronized, which indicates that the avalanche mass was integrated as a whole. After that, the velocities increased gradually, with maximum velocities appearing at 40–80 s. The speeds then gradually decreased, with the debris coming to a final rest after about 120 s. During the sliding process, particles in different layers on the same section accelerate and decelerate almost synchronously. However, velocities gradually decrease from the top layer (particles 3, 6, 9, and 12) to the bottom layer (particles 1, 4, 7, and 10). In addition, the velocities of particles at different parts of the same layer exhibit different characteristics. Particles in the rear of the landslide body (particles 1, 2, and 3) start slowly, and their movement continues for a short time. However, particles in the front of the landslide body (particles 10, 11, and 12) have a fast start, and their movement continues for a longer period. The simulated horizontal displacement of the monitored particles is illustrated in Fig. 13. Similar to the evolution laws of velocity, the runout distances of particles located at the front edge (particles 10, 11, and 12) are longer than those in the rear section (particles 1, 2, and 3), and the particles from the upper layers (particles 3, 6, 9, and 12) are able to travel longer runout distances than those from deeper layers (particles 1, 4, 7, and 10) in our simulations.

The momentum transfer model, i.e. an acceleration of the front blocks caused by increased collision (Okura et al. 2000), can be used to explain the results presented here. During the initial phase, the landslide body was integrated as a whole, so its movement was synchronized. Thereafter, the rock mass was fragmented into relatively small blocks. Because of the restricted free movement, collisions occurred between rock blocks. Rock blocks at the rear and bottom surfaces pushed rock blocks forward at the front and top surfaces. The collision interaction between the rock blocks involved the transfer of momentum, which caused the front of the mass to continue for a greater distance.

Parameters controlling the mobility of the Wenjiagou rock avalanche

Two major numerical parameters, the basal friction coefficient and the internal bonding strength, are the most crucial factors influencing landslide transport and deposition in the PFC2D model (Tang et al. 2009). This section describes a series of numerical simulations that were performed to investigate the runout distance and deposition area of the Wenjiagou rock avalanche in relation to the friction coefficient and bond strength (Figs. 14, 15).

Fig. 12 Velocity profiles of monitored particles versus time during landslide simulation

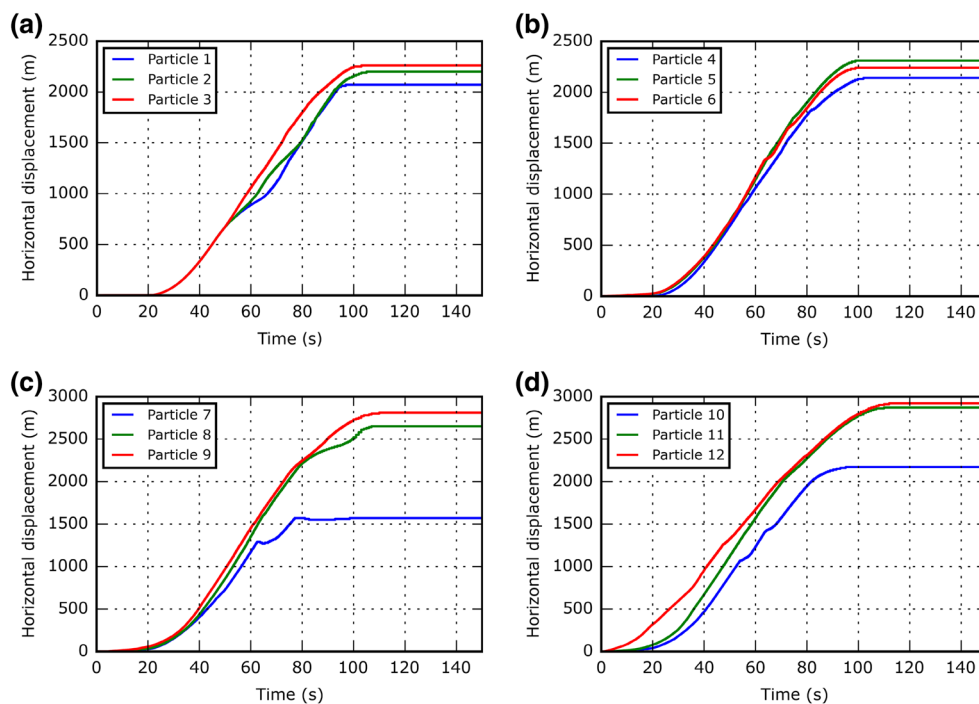
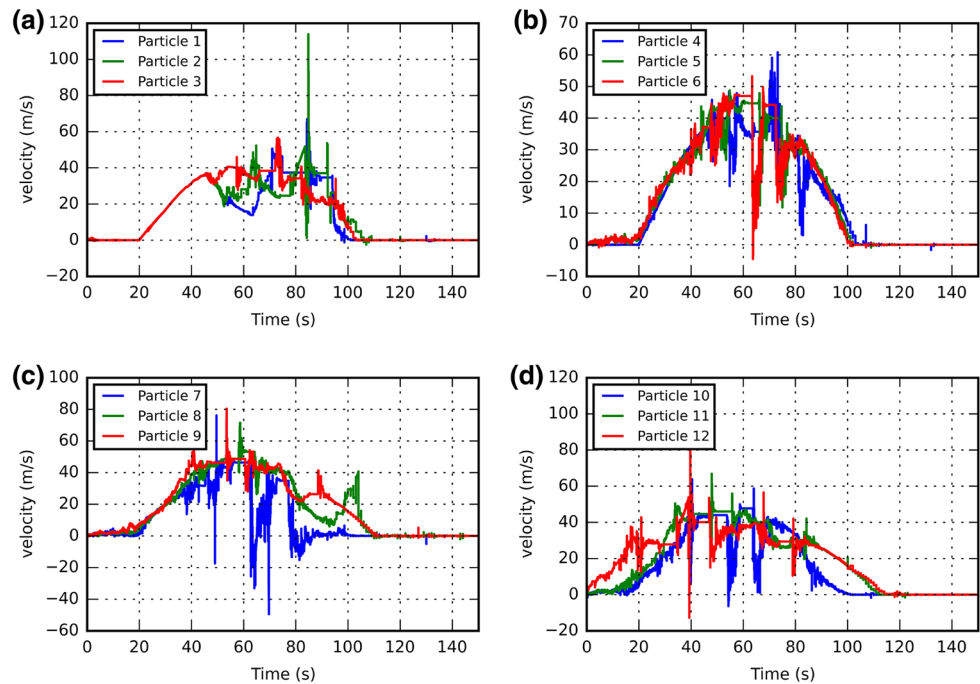


Fig. 13 The horizontal displacements of monitored particles versus time during landslide simulation

Influence of the friction coefficient

Kinetic friction occurs when the landslide body moves along the sliding surface. The kinetic friction coefficient is typically smaller than the static friction coefficient, which is crucial for conducting numerical simulations of a catastrophic avalanche. However, the kinetic friction

coefficient must be obtained experimentally and is difficult to measure accurately. Thus, in this study, a set of numerical experiments with basal coefficients of 0.2, 0.3, and 0.5 were carried out to determine the most plausible friction coefficient. Figure 14 presents the simulation results for the three friction coefficients of the avalanche slip surface.

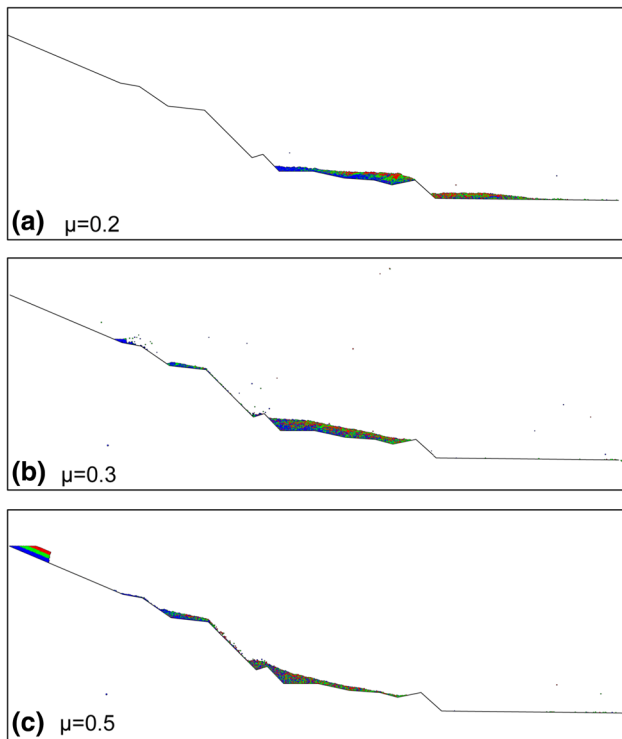


Fig. 14 Simulation results of sliding mass distributions under different residual friction coefficients ($C = 50$ Mpa)

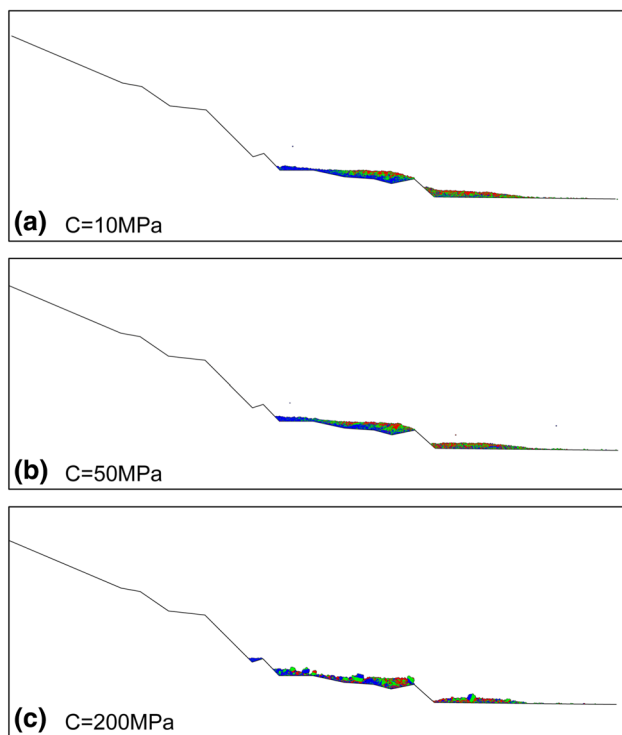


Fig. 15 Simulation results of sliding mass distributions under different bond strengths ($\mu = 0.2$)

As shown in Fig. 14, the basal friction coefficient strongly influences the runout distance and deposition patterns. The observed maximum travel distance of the Wenjiagou avalanche becomes shorter as the basal friction coefficient increases. In addition, the extent of the accumulation areas changes with the various basal friction coefficients. When the basal friction coefficient is assigned a value of 0.3, a small portion of the rock avalanche sediments is deposited at the Hanjia platform. With a friction coefficient of 0.5, no sliding occurs in portions of the rock mass, which remain on the rock avalanche source area.

The results of the simulation indicate that a low friction coefficient (about 0.2) satisfactorily accounts for the actual characteristics of the Wenjiagou avalanche. A small friction coefficient may be explained by a variety of reasons. Both sliding speed and magnitude of the load, in addition to factors such as the characteristics of the sliding surface, can affect the dynamic friction coefficient. In addition, air trapped in the zone between the sliding body and the valley bottom when the sliding body lands at a high velocity may cause debris avalanches to ride on a cushion of compressed air (Wang et al. 2010). Regardless of the theoretical explanation, low basal friction enables the debris avalanche to run several thousand metres in about 2 min, and at the same time, results in a rock avalanche with high velocity.

Influence of the bond strength

Bond strength values of 10, 50, and 100 MPa, indicating different levels of rock mass strength, were used to compare their effect on runout distance and deposition patterns. Figure 15 shows the results from multiple bond strength models with the basal friction coefficient ($\mu = 0.2$) as determined above. The series of simulation results indicate that lower bond strength enables the sliding body to more easily transform into a debris avalanche. High bond strength, on the other hand, will cause the main body mass to behave as a rigid block, thus making fragmentation difficult. In addition, it appears that the various parallel bond strength values used in this study do not make a significant difference in runout distance or debris flow avalanche deposit. With respect to the back analysis of the runout distance and debris morphology, bond strength of 50 Mpa and a basal friction coefficient of 0.2 gave the best simulation results for the Wenjiagou rock avalanche movement process.

Evolution of fragmentation

When stress exceeds the tensile/shear strength of the parallel bonds, cracks will form and propagate in the rock

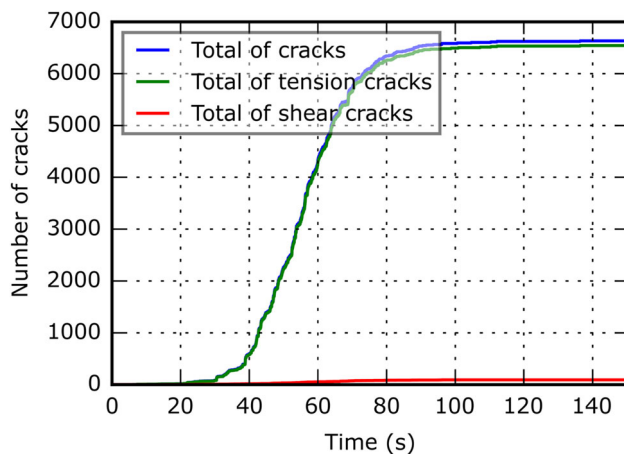


Fig. 16 Crack number time-history curves

mass, causing it to separate into blocks. Once the landslide begins to move, the bonds are rapidly destroyed because of the collision in rock fragmentation (Davies and McSaveney 2009). Figure 16 illustrates the crack numbers for parallel bonds during the Wenjiagou avalanche process.

According to the results, about 4 % (250) of the parallel bonds between particles were broken within 30 s, which indicates that cracks developed slowly. This was followed by a sharp increase in total number of cracks. During the interval from 30 to 70 s, the number of cracks increased by about 84 %, a substantial growth (Fig. 16), indicating almost complete breakage of the rock mass into granular debris. Based on the avalanche simulation (Fig. 11d), the mass of rock debris crashed into the bottom of the Wenjiagou valley during this time. Subsequently, the number of cracks remained at the same level. Figure 16 also shows that almost all of the cracks were generated by the tensile stress. Thus one could reasonably conclude that the collision of the rock mass with the valley bottom was the primary cause of the fragmentation of the Wenjiagou rock avalanche.

Energy analysis

To investigate the evolution of energy input and dissipation during the mass movement, various types of energy in incremental form were traced in our numerical model. Figure 17 shows the evolution of various incremental energy components against sliding time. The total energy in the granular system is determined by the combined effect of gravity and seismic forces. With regard to energy loss, there are essentially two types: energy dissipation resulting from collisions, and that caused by friction. The fluctuations in strain energy are very small, accounting for less than 1 % of the potential energy loss, and thus can be neglected in energy calculations. From the law of

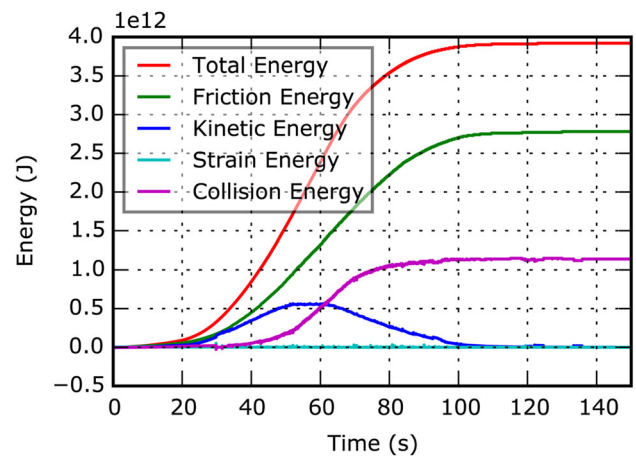


Fig. 17 Energy time-history curves

conservation of energy, the value of the total energy equals the sum of kinetic, collisional, and frictional energies. The results of the simulation show that the total energy was largely transformed into kinetic and frictional energy within the 0–40-s time interval. During the 40–80-s interval, the collision energy dissipation increased considerably. According to the simulation (Fig. 11d), the sliding body crashed into the bottom of the Wenjiagou Valley during this time. The kinetic energy development shows that the kinetic energy of the system was reduced to zero at about 120 s, as the Wenjiagou avalanche movement came to an end. Finally, the proportion of collisional and frictional energy had risen to 30 and 70 %, respectively. Therefore, it can be deduced that friction is the main source of energy dissipation during the entirety of the Wenjiagou avalanche movement.

High-mobility mechanism of the Wenjiagou rock avalanche

Based on numerical simulations, the hypermobility mechanism of the Wenjiagou rock avalanche will be discussed from an energy transformation perspective in this section.

High gravitational potential energy

The Wenchuan earthquake triggered the Wenjiagou rock avalanche and provided the sliding mass with a high initial speed. However, the main acceleration stage of the Wenjiagou avalanche was the projectile motion process. In this stage, almost all of the gravitational potential energy of the ejected body was converted into kinetic energy. The relative elevation of the avalanche was 1300 m, and the total volume of the avalanching mass was greater than $2.75 \times 10^7 \text{ m}^3$, which provided the moving mass with high gravitational potential energy. Thus the high gravitational

potential energy provided the energy basis for the high-speed and long-runout landslide.

Low basal friction coefficient

The basal friction coefficient from back analysis of the Wenjiagou avalanche event is abnormally low, which supports the argument for a substantial decrease in friction during the landslide process. The low coefficient of friction and resulting low energy loss facilitated the high-speed, long-distance movement of the rock mass.

Favourable movement of rock mass

Based on the simulation results, four types of mass movements can be distinguished during the Wenjiagou rock avalanche: sliding, falling, bouncing, and rolling. Diverse patterns of movement are accompanied by different forms of energy dissipation. Clearly, collision energy dissipation can contribute substantially to a reduction in avalanche runout distance. However, our simulation demonstrated that friction was the main source of energy dissipation, revealing that sliding and rolling were the dominant modes of movement during the Wenjiagou avalanche, and contributed to the high mobility.

Topographical conditions

Previous studies have suggested that the mass movement of rock avalanches is governed by topographical conditions (Dykes and Warburton 2007; Nishii and Matsuoka 2012; Sosio et al. 2008). Topographical conditions clearly play an important role in controlling the process of energy transformation. When an avalanche moves down a steep slope, its speed will increase, whereas when it moves over a gentle slope, its speed will be reduced. If the avalanching mass collides with a barrier, energy dissipation will occur, causing a reduction in runout distance. For the Wenjiagou rock avalanche, the free surface, steep terrain, and sufficient transport space provided the basic conditions for hypermobility.

Conclusions

The dynamic process of the Wenjiagou rock avalanche was simulated using PFC2D to analyse the mechanisms governing the high mobility of avalanche debris. The modelled scenario provided a satisfactory fit to the actual topography, adding credibility to the modelling results.

With regard to dynamic processes, the Wenjiagou rock avalanche can be divided into four phases: failure rupture, projectile motion, granular debris flow, and debris mass

accumulation. During the entire avalanche process, rock blocks at the front and upper edges exhibited higher mobility than those at the rear and bottom edges. The collision of the rock mass with the valley bottom was the main factor causing the fragmentation of the rock mass.

From a hypermobility perspective, the morphology of the sliding surface indicates that the basal friction coefficient has a larger influence than the bond strength on the maximum runout distance and debris morphology. In addition, friction was the main source of energy dissipation during the entirety of the Wenjiagou avalanche movement. Analysis results also indicate that the high gravitational potential energy was the basis for the high mobility. The low basal friction coefficient, favourable block movement, and topographical conditions all affected energy dissipation and contributed to the hypermobility of the Wenjiagou rock avalanche.

Acknowledgments This work was supported by the National Natural Science Foundation of China (grant nos. 41272298 and 41372290).

References

- Ayotte D, Hungr O (2000) Calibration of a runout prediction model for debris-flows and avalanches. In: Proceedings of the 2nd international conference on debris-flow hazards mitigation: mechanics, prediction, and assessment. Taipei, Taiwan, pp 505–514
- Cundall P (1971) A computer model for simulating progressive, large-scale movements in blocky rock systems. In: Proceedings of international symposium on rock fracture, pp 11–18
- Cundall PA, Strack OD (1979) A discrete numerical model for granular assemblies. *Geotechnique* 29:47–65
- Davies TR (1982) Spreading of rock avalanche debris by mechanical fluidization. *Rock Mech* 15:9–24
- Davies T, McSaveney M (2009) The role of rock fragmentation in the motion of large landslides. *Eng Geol* 109:67–79
- Davies T, McSaveney M, Hodgson K (1999) A fragmentation-spreading model for long-runout rock avalanches. *Can Geotech J* 36:1096–1110
- Deline P (2009) Interactions between rock avalanches and glaciers in the Mont Blanc massif during the late Holocene. *Quat Sci Rev* 28:1070–1083
- Dufresne A, Davies T (2009) Longitudinal ridges in mass movement deposits. *Geomorphology* 105:171–181
- Dykes AP, Warburton J (2007) Mass movements in peat: a formal classification scheme. *Geomorphology* 86:73–93
- Eisbacher G (1979) Cliff collapse and rock avalanches (sturzstroms) in the Mackenzie Mountains, northwestern Canada. *Can Geotech J* 16:309–334
- Erismann T (1979) Mechanisms of large landslides. *Rock Mech* 12:15–46
- Giani GP (1992) *Rock slope stability analysis*. Balkema, Rotterdam
- Havenith H-B, Strom A, Jongmans D, Abdrakhmatov A, Delvaux D, Tréfois P (2003) Seismic triggering of landslides, part A: field evidence from the Northern Tien Shan. *Nat Hazards Earth Syst Sci* 3:135–149
- Hoek E (1994) Strength of rock and rock masses. *ISRM News J* 2:4–16

- Hoek E, Diederichs MS (2006) Empirical estimation of rock mass modulus. *Int J Rock Mech Min Sci* 43:203–215
- Hoek E, Carranza-Torres C, Corkum B (2002) Hoek-Brown failure criterion—2002 edition. *Proc NARMS-Tac* 1:267–273
- Hsü KJ (1975) Catastrophic debris streams (sturzstroms) generated by rockfalls. *Geol Soc Am Bull* 86:129–140
- Huang Y, Zhang W-J, Xu Q, Xie P, Hao L (2012) Run-out analysis of flow-like landslides triggered by the Ms 8.0 2008 Wenchuan earthquake using smoothed particle hydrodynamics. *Landslides* 9:275–283
- Huang H-Q, Zhao Q-H, Li X-L (2015a) The analysis of dynamics characteristics of large-scale wenjiagou landslide-sturzstrom triggered by wenchuan earthquake. In: Lollino G, Giordan D, Crosta BG, Corominas J, Azzam R, Wasowski J, Sciarra N (eds) *Engineering geology for society and territory*, vol 2. *Landslide processes*. Springer International Publishing, Cham, pp 697–702
- Huang Y, Cheng H-L et al (2015b) SPH-based numerical simulation of catastrophic debris flows after the 2008 Wenchuan earthquake. *Bull Eng Geol Environ* 74:1137–1151
- Hungr O, Evans S, Bovis M, Hutchinson J (2001) A review of the classification of landslides of the flow type. *Environ Eng Geosci* 7:221–238
- Kent P (1966) The transport mechanism in catastrophic rock falls. *J Geol* 74:79–83
- Knapp S, Mamot P, Krautblatter M (2015) The mobility of rock avalanches: disintegration, entrainment and deposition—a conceptual approach. In: EGU general assembly conference abstracts, vol 17. EGU2015-12496. EGU General Assembly, Vienna
- Legros F (2002) The mobility of long-runout landslides. *Eng Geol* 63:301–331
- Liang Y (2014) Study on Wenjiagou landslide characteristics based on remote sensing image. Dissertation, China University of Geosciences (Beijing) (in chinese)
- Lo C-M, Lin M-L, Tang C-L, Hu J-C (2011) A kinematic model of the Hsiaolin landslide calibrated to the morphology of the landslide deposit. *Eng Geol* 123:22–39
- Lo C-M, Lee C-F, Chou H-T, Lin M-L (2014) Landslide at Su-Hua highway 115.9k triggered by Typhoon Megi in Taiwan. *Landslides* 11:293–304
- Lu C-Y, Tang C-L, Chan Y-C, Hu J-C, Chi C-C (2014) Forecasting landslide hazard by the 3D discrete element method: a case study of the unstable slope in the Lushan hot spring district, central Taiwan. *Eng Geol* 183:14–30
- Nicoletti PG, Sorriso-Valvo M (1991) Geomorphic controls of the shape and mobility of rock avalanches. *Geol Soc Am Bull* 103:1365–1373
- Nishii R, Matsuoka N (2012) Kinematics of an alpine retrogressive rockslide in the Japanese Alps. *Earth Surf Proc Land* 37:1641–1650
- Okura Y, Kitahara H, Sammori T, Kawanami A (2000) The effects of rockfall volume on runout distance. *Eng Geol* 58:109–124
- Poisel R, Roth W (2004) Run out models of rock slope failures. *Felsbau* 22:46–50
- Poisel R, Preh A, Hungr O (2008) Run out of landslides—continuum mechanics versus discontinuum mechanics models. *Geomech Tunn* 1:358–366
- Potyondy D, Cundall P (2004) A bonded-particle model for rock. *Int J Rock Mech Min Sci* 41:1329–1364
- Saiang D (2008) Determination of specific rock mass failure envelope via PFC and its subsequent application using FLAC. In: *Proceedings of the 1st international FLAC/DEM symposium on numerical modelling*, Minneapolis, USA. Itasca Consulting Group
- Shreve RL (1966) Sherman landslide, Alaska. *Science* 154:1639–1643
- Sosio R, Crosta GB, Hungr O (2008) Complete dynamic modeling calibration for the Thurwieser rock avalanche (Italian Central Alps). *Eng Geol* 100:11–26
- Stead D, Eberhardt E, Coggan J (2006) Developments in the characterization of complex rock slope deformation and failure using numerical modelling techniques. *Eng Geol* 83:217–235
- Tang C-L, Hu J-C, Lin M-L, Angelier J, Lu C-Y, Chan Y-C, Chu H-T (2009) The Tsaoling landslide triggered by the Chi-Chi earthquake, Taiwan: insights from a discrete element simulation. *Eng Geol* 106:1–19
- Tang Y, Zhang Z, Wang C, Zhang H, Wu F, Liu M (2015) Characterization of the giant landslide at Wenjiagou by the insar technique using TSX-TDX CoSSC data. *Landslides* 12:1015–1021
- Thompson N, Bennett MR, Petford N (2009) Analyses on granular mass movement mechanics and deformation with distinct element numerical modeling: implications for large-scale rock and debris avalanches. *Acta Geotech* 4:233–247
- Wang T, Shi J-S, Wu S-R, Zhang Y-S, Li B, Xin P, Sun P (2010) Formation mechanism of Wenjiagou high speed and long runout debris avalanche triggered by Wenchuan earth quake. *J Eng Geol* 18:631–644 (in Chinese)
- Wu S-R, Wang T et al (2010) Study on catastrophic landslides triggered by 2008 Great Wenchuan Earthquake, Sichuan, China. *J Eng Geol* 18:145–159 (in Chinese)
- Yin Y, Wang F, Sun P (2009) Landslide hazards triggered by the 2008 Wenchuan earthquake, Sichuan, China. *Landslides* 6:139–152
- Yuan R-M, Xu X-W, Chen G-H, Tan X-B, Klinger Y, Xing H-L (2010) Ejection landslide at northern terminus of Beichuan rupture triggered by the 2008 Mw 7.9 Wenchuan earthquake. *Bull Seismol Soc Am* 100:2689–2699
- Yuan R-M, Tang C-L, Hu J-C, Xu X-W (2014) Mechanism of the Donghekou landslide triggered by the 2008 Wenchuan earthquake revealed by discrete element modeling. *Nat Hazards Earth Syst Sci* 14:1195–1205
- Zhang M, Yin Y-P (2013) Dynamics, mobility-controlling factors and transport mechanisms of rapid long-runout rock avalanches in China. *Eng Geol* 167:37–58
- Zhang M, Yin Y-P, Wu S-R, Zhang Y-S, Han J-L (2011) Dynamics of the Niumiangou Creek rock avalanche triggered by 2008 Ms 8.0 Wenchuan earthquake, Sichuan, China. *Landslides* 8:363–371
- Zhang M, Yin Y-P, McSaveney M (2016) Dynamics of the 2008 earthquake-triggered Wenjiagou Creek rock avalanche, Qingping, Sichuan, China. *Eng Geol* 200:75–87
- Zhou J-W, Cui P, Fang H (2013) Dynamic process analysis for the formation of Yangjiagou landslide-dammed lake triggered by the Wenchuan earthquake, China. *Landslides* 10:331–342
- Zhou J-W, Huang K-X, Shi C, Hao M-H, Guo C-X (2015) Discrete element modeling of the mass movement and loose material supplying the gully process of a debris avalanche in the Baiy Gully, Southwest China. *J Asian Earth Sci* 99:95–111